

UNCLASSIFIED

~~CONFIDENTIAL~~

COPY NO.
RM No. E8F07

SEP 21 1947

~~2-6-3~~



~~ft~~
1077

RESEARCH MEMORANDUM

DESIGN AND PERFORMANCE OF EXPERIMENTAL AXIAL-DISCHARGE
MIXED-FLOW COMPRESSOR

II - PERFORMANCE OF IMPELLER

By Ward W. Wilcox

Flight Propulsion Research Laboratory
Cleveland, Ohio

CLASSIFICATION CANCELLED

Authority NACA R7 2385 Date 8/18/54

CLASSIFIED DOCUMENT

By ANTA 9/1/54

This document contains classified information affecting the National Defense of the United States within the meaning of the Espionage Act, USC 5014 and 5018. Its transmission or the revelation of its contents in any manner to an unauthorized person is prohibited by law. Information so classified may be imparted only to persons in the military and naval services of the United States, appropriate civilian officers and employees of the Federal Government who have a legitimate interest therein, and to United States citizens of known loyalty and discretion who of necessity must be informed thereof.



NATIONAL ADVISORY COMMITTEE FOR AERONAUTICS

WASHINGTON
August 12, 1948

UNCLASSIFIED

~~CONFIDENTIAL~~

NACA LIBRARY
LANGLEY MEMORIAL AERONAUTICAL
LABORATORY
Langley Field, Va.



NATIONAL ADVISORY COMMITTEE FOR AERONAUTICS

RESEARCH MEMORANDUM

DESIGN AND PERFORMANCE OF EXPERIMENTAL AXIAL-DISCHARGE

MIXED-FLOW COMPRESSOR

II - PERFORMANCE OF IMPELLER

By Ward W. Wilcox

SUMMARY

An axial-discharge mixed-flow compressor was designed to combine the compactness, reliability, and wide operating range of a mixed-flow compressor with the high flow capacity per unit of frontal area that characterizes the axial-flow compressor. The primary objective was to maximize the flow capacity for a pre-determined pressure ratio. The impeller was operated over the obtainable range of equivalent weight flows at equivalent impeller tip speeds varying from 1000 to 1480 feet per second.

At the design tip speed of 1480 feet per second, a maximum flow capacity of 18.7 pounds per second, a peak total-pressure ratio of 3.7, and a peak adiabatic efficiency of 0.78 were obtained. The flow capacity per unit of frontal area for this axial-discharge impeller is much greater than that of commercial mixed-flow compressors for which data are now available but is somewhat less than that for the commercial axial-flow compressors having the highest flow capacity per unit of frontal area. The maximum weight-flow value reported herein is considered conservative because the limitation of flow occurs in the experimental setup rather than in the impeller itself.

INTRODUCTION

Turbojet and turbine-propeller aircraft engines require compact, dependable compressors of high mass flow capacity. In the design of the axial-discharge mixed-flow impeller (reference 1), an effort was made to combine the compactness, simplicity, and reliability of a centrifugal compressor with the high flow capacity per unit of frontal area of the axial-flow compressor. In this impeller, the compression was accomplished in a rotor of high blade solidity and work output; the air entering and leaving the rotor had no radial component of motion. A limiting outside diameter of 14 inches was

arbitrarily selected and an inlet tip diameter of 11.25 inches was determined from maximum flow considerations. At the design tip speed of 1480 feet per second, the over-all total-pressure ratio was calculated to be 3.51 and the equivalent weight flow, 19.7 pounds per second.

A cascade of airfoil sections was used to establish the desired prerotation at the impeller inlet. Separate flow tests were made to determine the turning angle and velocity distribution of the air behind these vanes. Both the impeller and the cascade of vanes were fabricated and tested at the NACA Cleveland laboratory.

In order to determine the impeller performance characteristics without diffuser limitations, the impeller and the prerotation vanes were installed in a special setup. The investigation covered the obtainable range of weight flows at equivalent tip speeds from 1000 to 1480 feet per second. Over-all performance was evaluated from extensive surveys of the flow conditions at the impeller discharge.

APPARATUS AND PROCEDURE

Axial-discharge impeller. - A photograph of the impeller, partly installed in the test rig is shown in figure 1. An axial cross section of the impeller passage, as well as the angular variation of the blade tip along the flow path through the impeller, is shown in figure 2. The accompanying table shows that the outer radius increases from 5.585 inches to 6.960 inches and the inner radius increases from 2.750 inches at the inlet to 5.900 inches at the outlet. This radial increase and the change in angle ϕ along the axis of rotation indicate that the mean flow path has a continuous increase in both radius of rotation and angular velocity from entrance to exit of the impeller. A radial clearance of 0.040 inch was maintained between the blade tip and the outer casing at all axial stations. Because the blade section was asymmetrical about a radial line through the tip, the root and tip dimensions are given with figure 2.

The impeller blank was constructed in two sections from SAE 4340 steel with a cut-out between sections to reduce weight and thus decrease hub stresses. After the two sections were bolted together, the 18 thin, highly cambered blades were machined from the composite piece.

The prerotation vanes are sections of the NACA 65-1210 airfoil cast in brass by the lost-wax process. The chord was held constant at 1.75 inches and the air was turned by varying the angle of attack from hub to tip. The trailing edges of these blades were about 1/4 inch upstream of the impeller face.

Experimental setup. - In order to determine the performance characteristics of the axial-discharge impeller without the limitations imposed by a diffuser, the impeller was installed in a special rig (fig. 3). The inlet section of the rig was directly connected to the laboratory refrigerated-air supply by 12 diameters of 13-inch pipe. The impeller discharged the air into a straight annulus 24 inches long, from which the air passed into a baffled collector. Two collector outlet pipes led directly to the laboratory altitude-exhaust system. In order to minimize heat transfer, the inlet pipe was lagged with 4 inches of Fiberglas insulation and then covered with heavy paper, tar, and asbestos cement. The impeller housing and the discharge annulus were covered with 3 inches of magnesia insulation.

The impeller was mounted with one spherically-seated front journal bearing and three spherically-seated rear journal bearings. A balance piston was used to reduce the load on the two opposing thrust bearings in front of the impeller. One side of the balance-piston chamber was vented to the impeller outlet and the other to the inlet pipe and thus the balance was automatically maintained for all changes in over-all pressure ratio.

The impeller was driven by a 2500-horsepower induction motor through a variable-slip magnetic coupling and speed increasers with an over-all speed ratio of 17.96:1. Constant speed was maintained within $\pm 1/2$ percent by means of an electronic control that regulated the slip of the magnetic coupling.

Prerotation-vane rig. - A wooden mock-up of the inlet section with an inner and outer diameter corresponding to those at the impeller inlet was used to check the turning angles through the prerotation vanes. Ambient air was drawn through a bellmouth, turned by the vanes, and then discharged to the laboratory altitude-exhaust system. Radial and circumferential surveys of the turning angle downstream of the vanes were made with a standard claw-type yaw tube in a plane corresponding to the impeller inlet.

Instrumentation. - Air weight flow was measured by a submerged variable-area orifice meter in the inlet pipe. Inlet conditions were measured in the inlet pipe at a plane 4 diameters upstream of the impeller. Total pressure was measured by two pitot tubes and static pressure, by two wall orifices. Inlet temperature was measured by two calibrated iron-constantan thermocouples connected to a self-balancing potentiometer. All inlet instruments were installed as specified in reference 2. Duplicate instruments were installed downstream of the balance-piston vent in the inlet pipe

and observations from these instruments, in conjunction with velocity measurements in the vent line, proved that the air leakage past the balance-piston seal was insignificant.

Impeller-outlet flow measurements were taken in a plane 1/4 inch downstream of the impeller discharge (fig. 3). Because of the supersonic velocities at this location, special instrument techniques were required. Radial surveys of flow angle, total pressure, and total temperature were made at the peripheral positions shown in figure 4; wall static-pressure taps were located on both the inner and outer annulus walls; and a linear radial variation of static pressure was assumed. The discharge survey instruments were 1/4 inch in diameter and could be completely withdrawn from the flow passage during static-pressure observations. Because the discharge flow was supersonic at all conditions investigated, the static pressure downstream of the instruments was always affected by their presence in the airstream. In addition, many other static-pressure taps were placed along the impeller outer shroud and along both the inside and outside walls of the annular passage.

Total pressure and flow angle were measured with a three-hole cylindrical yaw tube. In general, the angular sensitivity of the instrument was greater than the accuracy of its alinement with the axis of rotation. Over-all accuracy of the angle determination was within 1°. At supersonic velocity, a normal shock was assumed to exist immediately in front of the total-pressure tube. For one-dimensional flow, the relation between the free-stream Mach number and the ratio of total pressure behind a normal shock to the total pressure in the free stream is given by

$$\frac{P_1}{P_0} = \left(\frac{7M_0^2 - 1}{6} \right) \left(\frac{36M_0^2}{35M_0^2 - 5} \right)^{3.5} \left(\frac{1}{1 + 0.2M_0^2} \right)^{3.5}$$

where

P_1 total pressure behind normal shock

P_0 total pressure in free stream

M_0 Mach number in free stream

By successive approximations, the true total pressure P_0 may be found from this equation when the observed total pressure P_1 and the static pressure (hence Mach number) are known. Calibration of

this instrument showed that the angle sensitivity and corrected total pressure were satisfactory for Mach numbers up to 2.0. Discharge-pressure measurements are estimated to be accurate within ± 1 percent and discharge Mach numbers, within ± 2 percent.

The temperature-survey probe was a semishielded iron-constantan thermocouple of the type described in reference 3. This thermocouple was calibrated for Mach numbers up to 2.0 and was found to have a very high recovery factor at all values. A self-balancing potentiometer was calibrated for use with this thermocouple.

Experimental procedure. - Compressor performance data were obtained over the range of obtainable equivalent weight flows $W \sqrt{\theta/\delta}$ (where W is weight flow in lb/sec, θ is the ratio of inlet temperature to NACA standard sea-level temperature, and δ is the ratio of inlet pressure to NACA standard sea-level pressure) at constant values of equivalent tip speed $U/\sqrt{\theta}$ (where U is the impeller tip speed in ft/sec) in a range from 1000 to 1480 feet per second. Inlet-air conditions were maintained at a pressure of 15 inches of mercury absolute and a temperature of about 0° F. The low pressure was necessitated by power and refrigerated-air limitations. Because of the low temperature, the necessary equivalent tip speeds were possible at lower actual speeds, which helped to keep the bearing-temperature and stress conditions within reasonable limits.

For a given weight flow and speed, the static pressures along the impeller casing and the inlet static pressures were photographically recorded with the discharge-survey instruments completely withdrawn from the stream. The surveys of temperature and pressure at the impeller discharge were then made, with the instruments remotely controlled by means of motorized actuators.

RESULTS AND DISCUSSION

Flow distribution at impeller inlet. - A comparison of the turning angles ψ at the outlet of the prerotation vanes and the design flow angle at the impeller inlet is shown in figure 5. The turning angles were, in general, 1° higher than the design values. A large decrease in turning angle near the hub was principally due to clearance between the vane tips and the hub. With the exception of the boundary layers on the inner and outer walls, however, the distribution of turning angles is very close to that for design. Design angles between the impeller blades and the relative entering-air velocities will therefore be obtained at a flow slightly lower than the design value.

Flow distribution at impeller outlet. - Complete flow-distribution patterns at the impeller outlet were required to evaluate the impeller performance and to form a basis for a supersonic-diffuser design. Although many surveys were made for a wide range of flow conditions, the principal trends can be shown by survey results for the maximum-flow, minimum-flow, and flow for peak-efficiency conditions at the design equivalent tip speed of 1480 feet per second. The radial variation of flow angle β (angle between flow direction and the axial direction) is given in figure 6(a). A complete change in the general trend is evident between maximum and minimum flow. At the minimum flow condition, the discharge air angle decreased quite uniformly from 86° near the inner wall to 69° near the outer wall. However, at maximum flow, the trend is reversed with an increase from 55° to 64° for the same variation in radius. At the peak-efficiency flow condition, the total variation in flow angle from wall to wall is only 3° .

The variation of Mach number with radius is presented in figure 6(b) for the same representative flows. The Mach number decreases with increasing radius at maximum flow, reverses the trend at minimum flow, and is nearly constant across the passage for the peak-efficiency condition. In general, the boundary layer appears to be thicker at the outer wall than on the inner wall, which is probably caused by an impeller-tip-clearance effect and a greater axial distance from impeller tip to measuring station at the outer wall. The nearly constant profiles of both flow angle and Mach number at the peak-efficiency flow considerably simplify the design of a supersonic diffuser.

For all flows, the tangential velocity increases with increasing radius and exhibits a thick boundary layer near the outer wall, as shown in figure 6(c). The tangential-velocity distribution is approximately a wheel-type rotation, as would be expected from the impeller geometry. The variation of axial velocity with radius is presented in figure 6(d). At maximum flow, the axial velocity is high near the inner wall and low near the outer wall of the annulus. For minimum flow, this variation is reversed; that is, the axial velocity is very low near the inner wall and increases rapidly with increasing radius. The flow distribution across the passage is quite uniform at peak efficiency.

The flow-distribution characteristics of this impeller may be summarized as follows: At high flows the flow concentrates near the inner wall, at low flows near the outer wall, and for peak efficiency the flow distribution is uniform across the passage.

Impeller performance. - In order to evaluate the performance of this impeller in terms of commonly used parameters, the total-temperature and total-pressure distributions at the impeller discharge must be determined and analyzed. Figure 7(a) presents the variation with radius of the temperature rise through the impeller for the three representative flows at design speed. Temperature rise is a measure of the energy addition by the impeller and, as was indicated by the tangential-velocity pattern (fig. 6(c)), the energy addition increases with increasing radius. The existence of a clearance effect near the outer wall is also indicated by the temperature-rise curves.

The variation of total-pressure ratio with radius is shown in figure 7(b). The trend of these curves very closely follows that for the temperature rise. At maximum flow, the total-pressure-ratio curve levels off near the inner annulus wall. This phenomenon is also indicated by the configuration of the temperature-rise curve and the tangential-velocity curve (fig. 6(c)). At the rear inner shroud of the impeller, the blades turn slightly past the straight axial direction to give a slight forward sweep; and for this particular high-flow condition, the tendencies toward flow separation and increase in boundary layer in the impeller passages are sufficiently diminished to obtain full advantage of this blade characteristic.

By combining the survey data for total-pressure ratio and temperature rise, a point-to-point variation of adiabatic efficiency is obtained (fig. 7(c)). For the two higher flows, the efficiency decreases with increasing radius but, for the low-flow condition, the efficiency is low over the inner third of the passage and then essentially constant with radius. In general, however, the efficiency is highest over that part of the annulus handling most of the flow.

The over-all impeller performance is given in figure 8. The efficiency and pressure ratio are mass-weighted averages and, as such, do not penalize the impeller performance for any mixing losses incurred by nonuniform total-pressure or velocity distributions. This impeller has a comparatively large operating range at relatively constant total-pressure ratio, particularly at the lower tip speeds. Difficulty was experienced in accurately determining the surge point or low-flow limitation at all tip speeds because this impeller, in the installation used, had no discernible periodic pulsation even at extremely low flows. Flow conditions, however, did become sufficiently unsteady at these low flows to preclude the possibility of obtaining reliable data. The maximum equivalent flow at the design speed of 1480 feet per second was 18.7 pounds per second and

a peak pressure ratio of 3.7 was obtained. This performance was in close agreement with that predicted by theoretical design. The over-all mass-weighted efficiency of the impeller decreases with increasing tip speed. In general, the peak efficiency of 0.78 for this compressor at design speed is lower than that for good conventional impellers. Inasmuch as this impeller is the first model of a radical design, considerable improvement in efficiency might be obtained by design modifications.

There is strong evidence that the limitation of the maximum flow was due to the external ducting of the installation rather than to the impeller itself. From an investigation of the flow in the annular outlet section, it was found that thickening of the boundary layer and the reduction in air density accompanying flow losses caused the axial-velocity component to reach the sonic limitation at the exit of the annulus at a lower flow than that required to produce choking in the impeller. Absence of choking in the impeller is indicated in figure 9, in which the ratio of static pressure at the outer wall to inlet static pressure is plotted against axial distance along the flow path. At all flows, the rise in static pressure from the impeller inlet to outlet is uniform. The magnitude of the static-pressure rise is greatly affected by the static-pressure drop across the prerotation vanes. If choking conditions existed, a large drop in static-pressure ratio would be expected. Even at maximum flow, however, the curves of figure 9 do not show this characteristic of choking flow. Because of the extremely high resultant discharge velocities, the static-pressure ratio is much lower than the impeller total-pressure ratio.

The flow capacity per unit frontal area for this axial-discharge impeller is exceptionally high when compared with existing mixed-flow compressors. On the basis of equivalent impeller tip diameters, the axial-discharge impeller has a 36-percent larger flow capacity than the highest-capacity mixed-flow impeller reported to date (reference 4). On the basis of over-all compressor diameter, the axial-discharge impeller has an even greater flow capacity because the diffuser will be limited to the same over-all diameter as the impeller; whereas for the impeller reported on in reference 4, the diffuser diameter is considerably larger than the impeller diameter because of the radial component of velocity at the impeller discharge.

A comparison with unpublished data showed that the axial-discharge impeller, with its advantages of simplicity, reliability, and compactness, had only 25 percent less flow capacity per unit of frontal area than the best commercial axial-flow compressor.

SUMMARY OF RESULTS

From an initial investigation of the flow and performance characteristics of an experimental axial-discharge impeller, the following results were obtained:

1. By handling an equivalent weight flow of 18.7 pounds per second at a design tip speed of 1480 feet per second with an overall diameter of 14 inches, the axial-discharge impeller demonstrated a flow capacity per unit of frontal area greater than that of existing mixed-flow compressors. Because the limitation of flow occurred in the external flow system for this investigation, the flow capacity reported was conservative.

2. At the design tip speed of 1480 feet per second, a maximum total-pressure ratio of 3.7 and a peak adiabatic efficiency of 0.78 were obtained. The impeller exhibited a wide operating range at all tip speeds.

3. Because the axial-discharge impeller has only 18 long, highly cambered rotating blades, it was shown to be more reliable, simpler, and more compact than axial-flow compressors, but the flow capacity is less than that of axial-flow compressors of the same diameter.

4. The performance obtained was in close agreement with that predicted by the theoretical design.

Flight Propulsion Research Laboratory,
National Advisory Committee for Aeronautics,
Cleveland, Ohio.

REFERENCES

1. Goldstein, Arthur W.: Design and Performance of Experimental Axial-Discharge Mixed-Flow Compressor. I - Impeller Design Theory. NACA RM No. E8FO4, 1948.
2. NACA Subcommittee on Supercharger Compressors: Standard Procedures for Rating and Testing Centrifugal Compressors. NACA ARR No. E5F13, 1945.

3. Markowski, S. J., and Moffatt, E. M.: Instrumentation for the Development of Aircraft Power Plant Components Involving Fluid Flow. Paper presented before SAE Natl. Aero. Meeting (New York), April 9-11, 1947.
4. Ritter, William K., Ginsburg, Ambrose, and Redlitz, Alfred G.: Effects of Axial-Plane Curvature and Passage-Area Variation on Flow Capacity of Radial-Discharge Impeller with Conventional Inlet Buckets. NACA TN No. 1068, 1946.

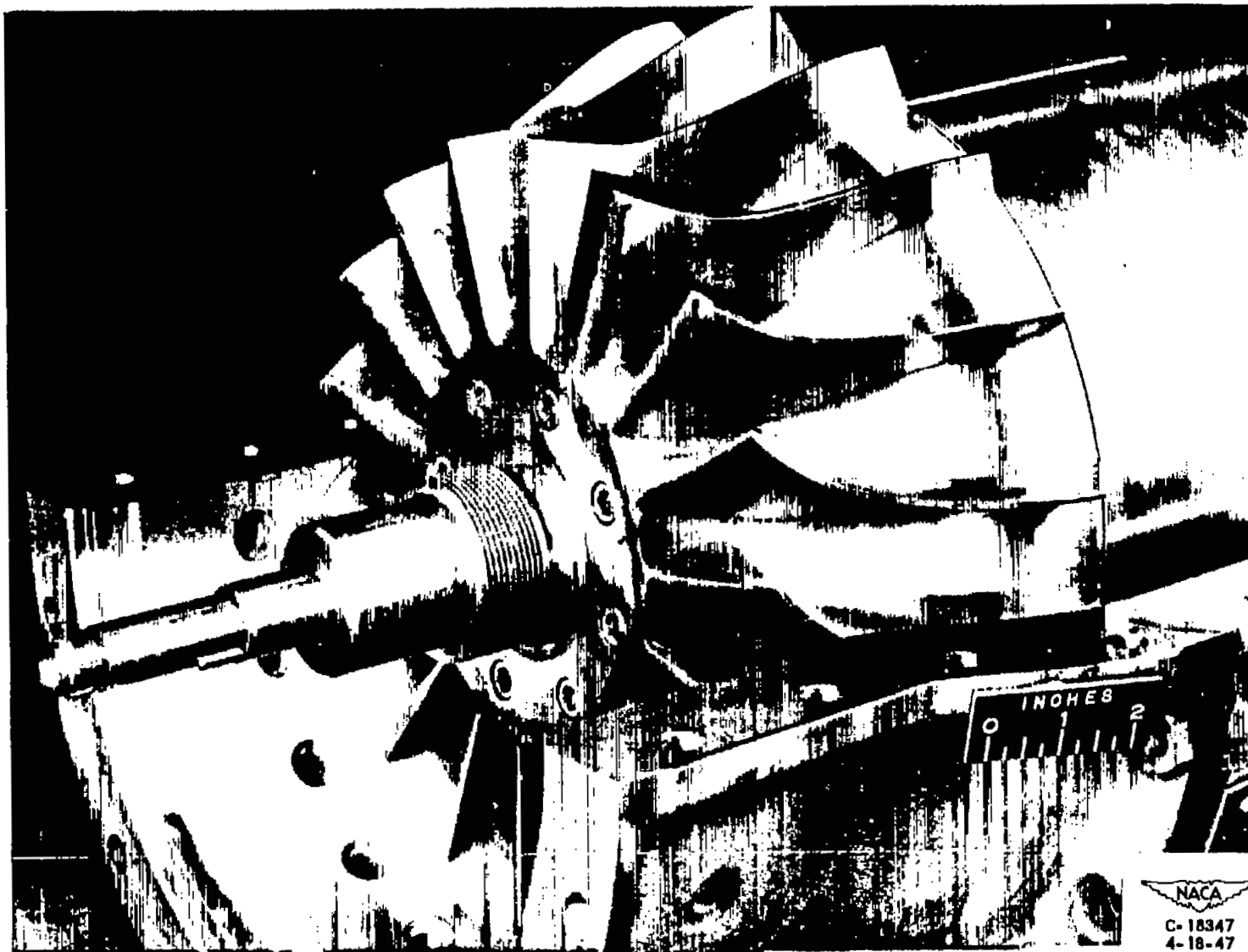
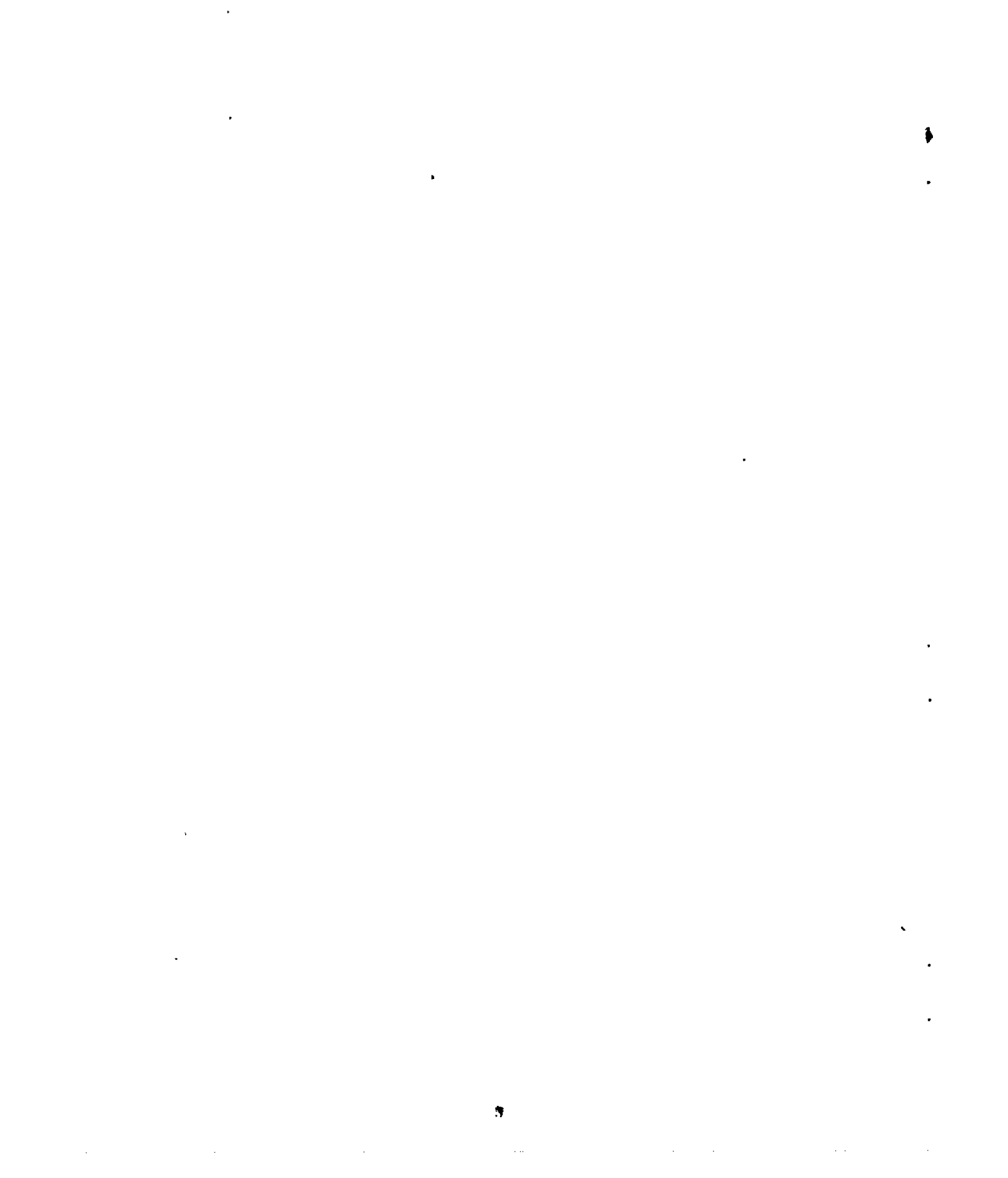
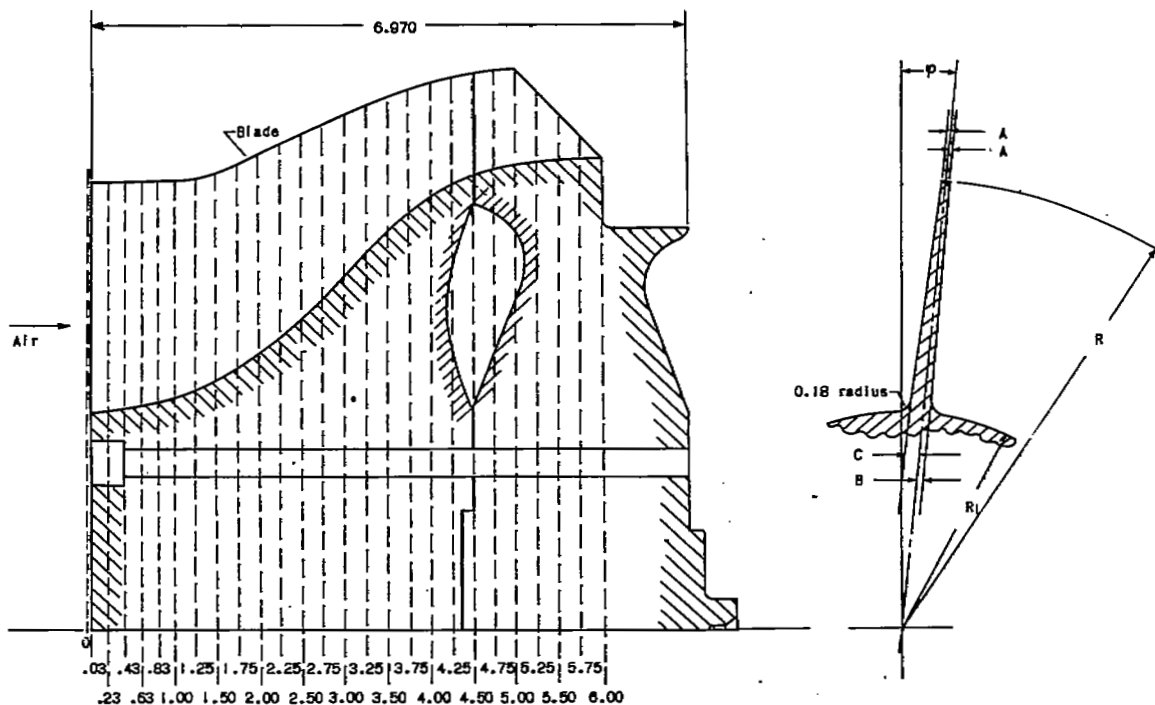


Figure 1. - Axial-discharge mixed-flow impeller partly installed in rig.



981



(a) Axial cross section.

(b) Typical blade section normal to axis.

Station along axis (in.)	R (in.)	R ₁ (in.)	A (in.)	B (in.)	C (in.)	P (deg)	(min)
0.03	5.785	2.750	0.048	0.232	-0.068	-0	30
.43	5.565	2.750	.044	.152	.064	1	53
.83	5.565	2.750	.040	.108	.106	3	45
1.25	5.565	2.750	.040	.092	.122	6	15
1.75	5.565	2.750	.037	.088	.120	6	37
2.25	5.565	2.750	.036	.090	.118	7	43
2.75	5.530	2.990	.036	.099	.108	9	06
3.25	5.710	3.118	.035	.100	.104	10	19
3.75	5.813	3.274	.032	.100	.100	11	20
4.25	5.818	3.455	.033	.100	.093	12	08
4.75	6.038	3.676	.033	.100	.088	12	51
5.25	6.158	3.928	.034	.094	.090	13	29
5.75	6.276	4.200	.032	.090	.095	14	05
6.00	6.381	4.470	.032	.086	.104	14	35
6.25	6.502	4.738	.032	.086	.104	14	58
6.50	6.607	4.985	.032	.048	.088	15	16
6.75	6.702	5.210	.032	.048	.090	15	33
7.00	6.784	5.396	.032	.054	.084	15	47
7.25	6.852	5.488	.030	.058	.079	15	59
7.50	6.904	5.568	.031	.050	.082	16	07
7.75	6.940	5.756	.031	.036	.090	16	12
8.00	6.960	5.818	.031	.026	.094	16	07
8.25	6.965	5.858	.032	.018	.095	15	52
8.50	6.430	5.882	.032	.010	.070	15	28
8.75	6.165	5.895	.032	.005	.064	14	47
9.00	5.900	5.900	.032	.032	.052	13	36



Figure 2. - Cross section of axial-discharge mixed-flow impeller. (All dimensions in inches.)

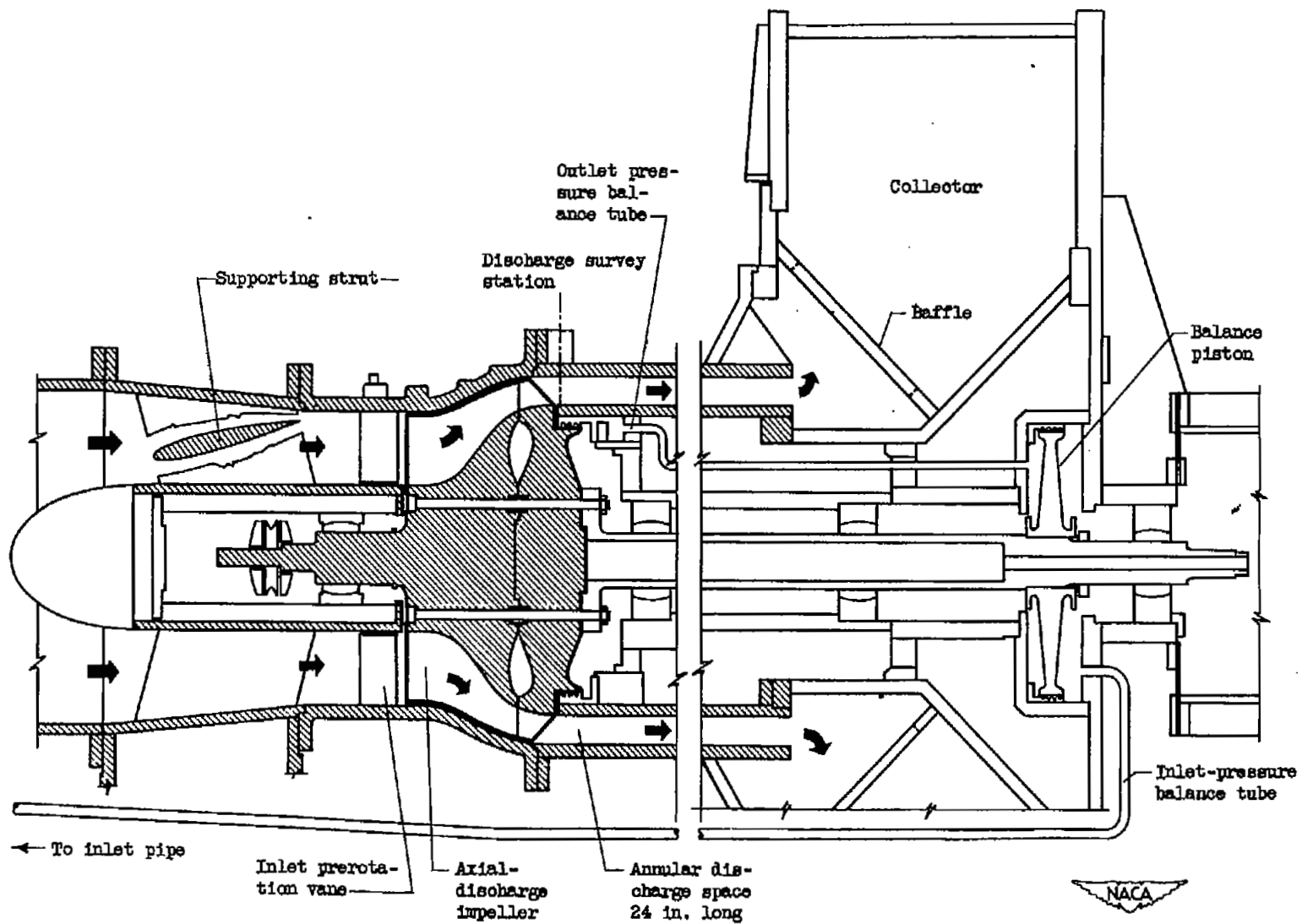


Figure 3. - Diagrammatic sketch of axial-discharge mixed-flow impeller installed in special rig.

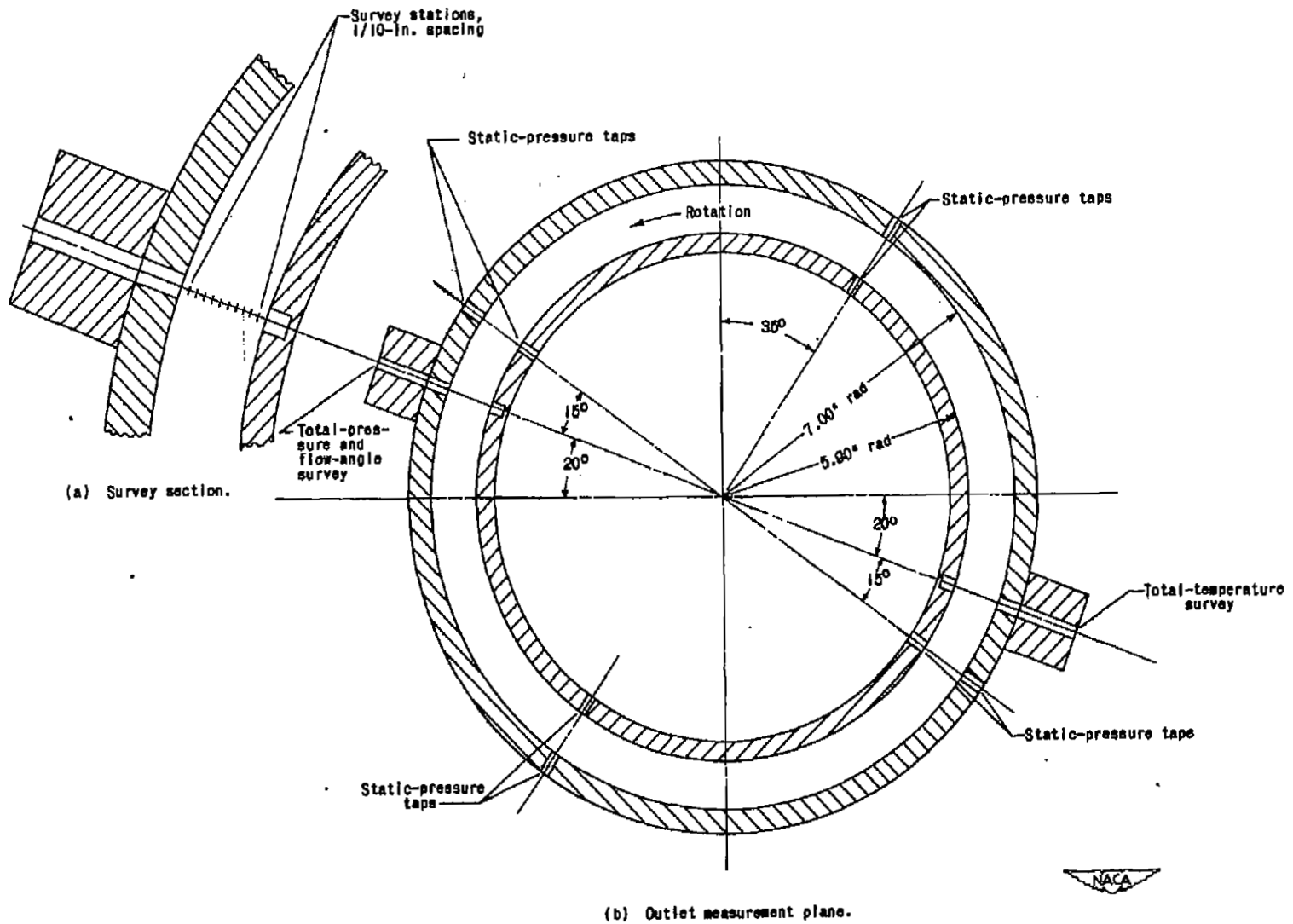


Figure 4. - Schematic diagram showing peripheral location of instruments at impeller outlet.

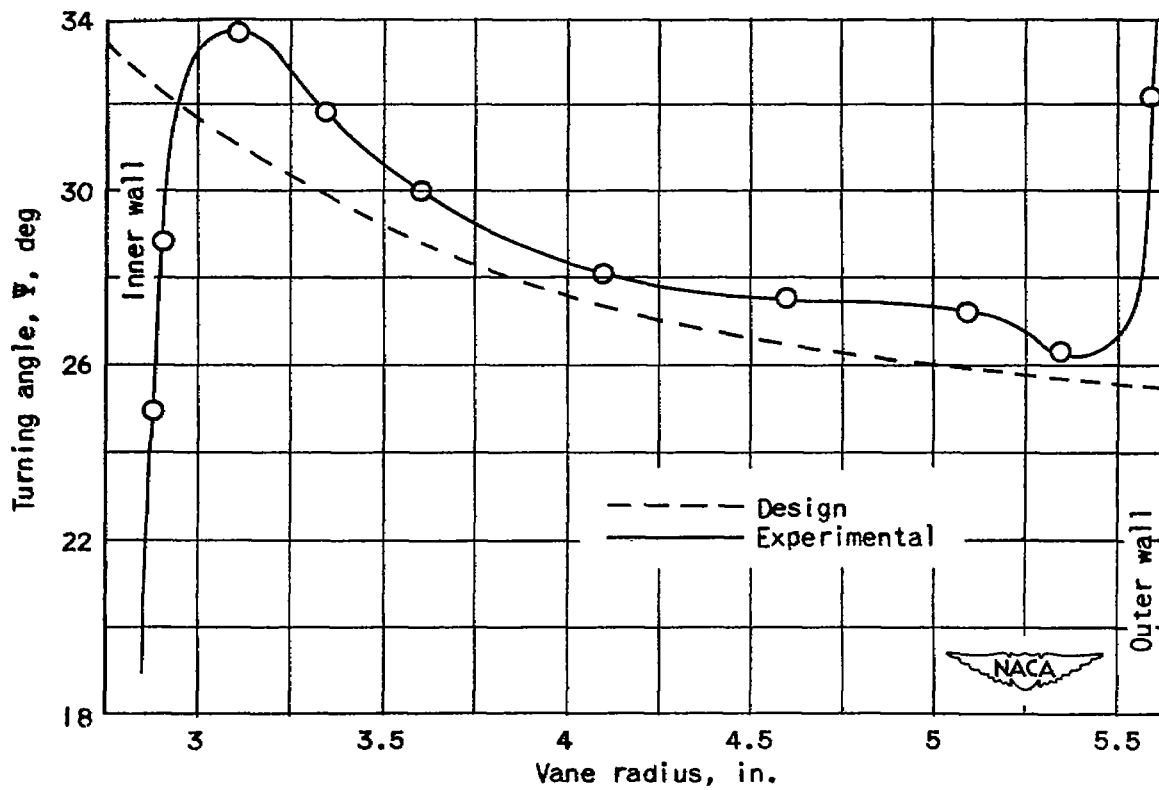
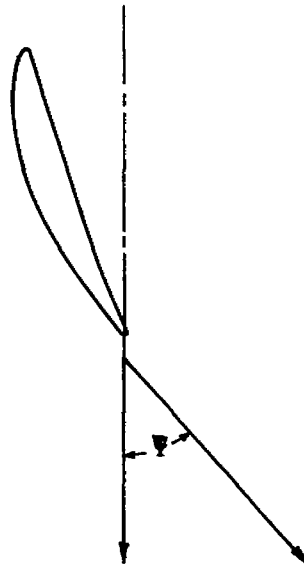
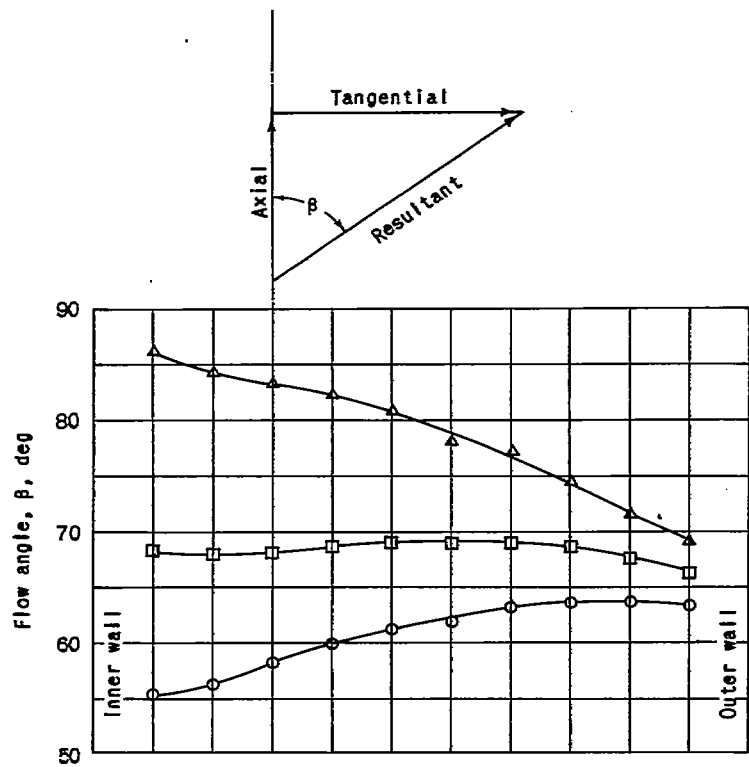
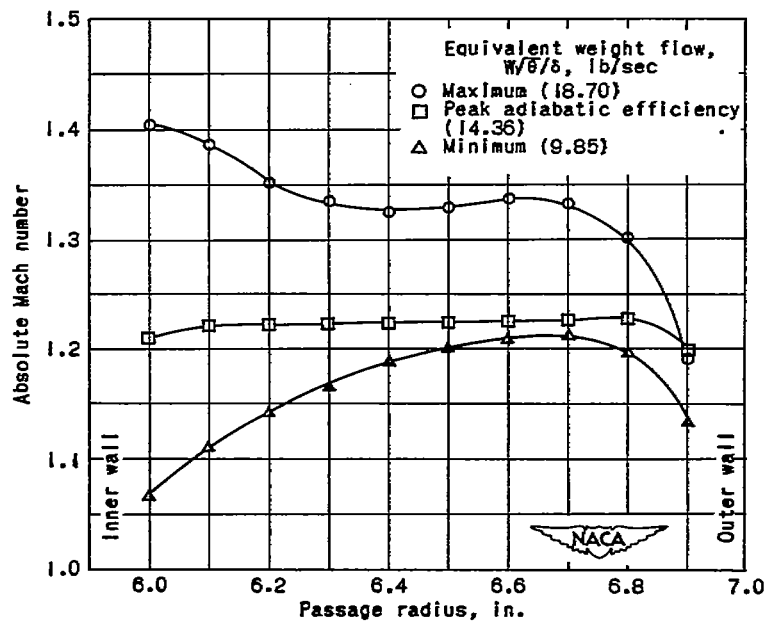


Figure 5. - Turning-angle distribution at outlet of prerotation vanes in axial-discharge mixed-flow impeller.

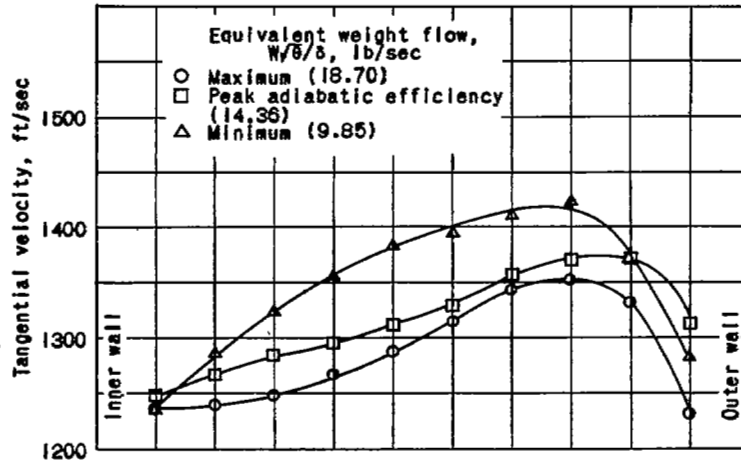


(a) Flow angle.

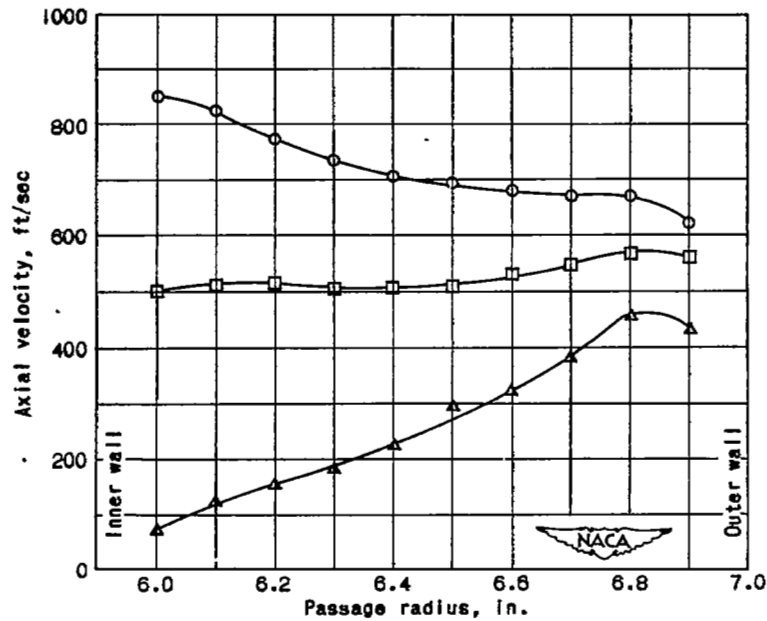


(b) Absolute Mach number.

Figure 6. - Flow distribution at impeller outlet for equivalent tip speed of 1480 feet per second.

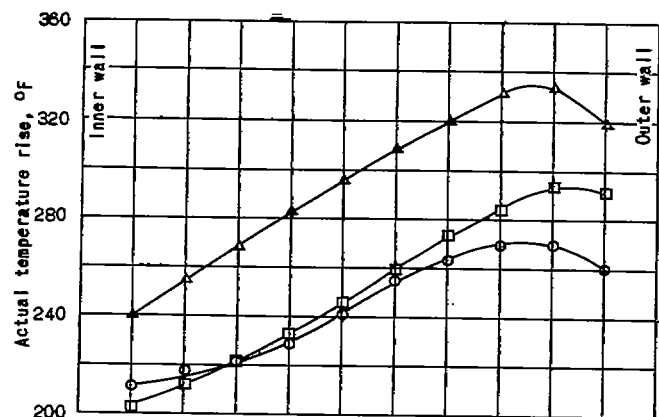


(c) Tangential velocity.

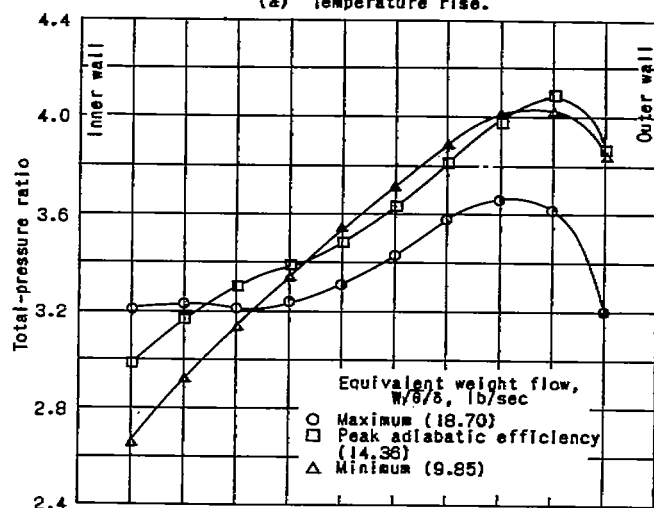


(d) Axial velocity.

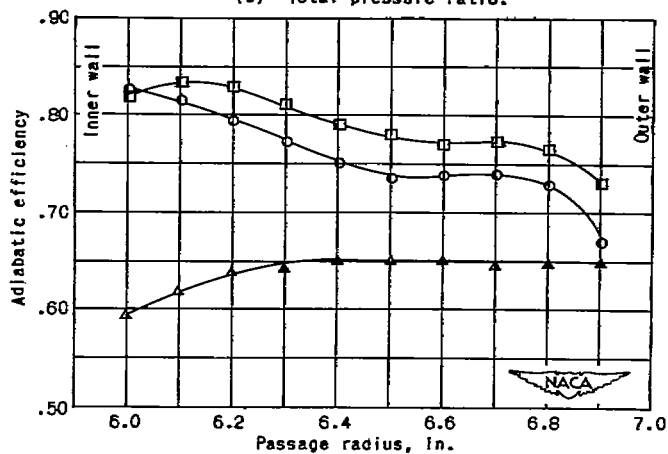
Figure 6. - Concluded. Flow distribution at impeller outlet for equivalent tip speed of 1480 feet per second.



(a) Temperature rise.



(b) Total-pressure ratio.



(c) Adiabatic efficiency.

Figure 7. - Performance at outlet of axial-discharge mixed-flow impeller at equivalent tip speed of 1480 feet per second.

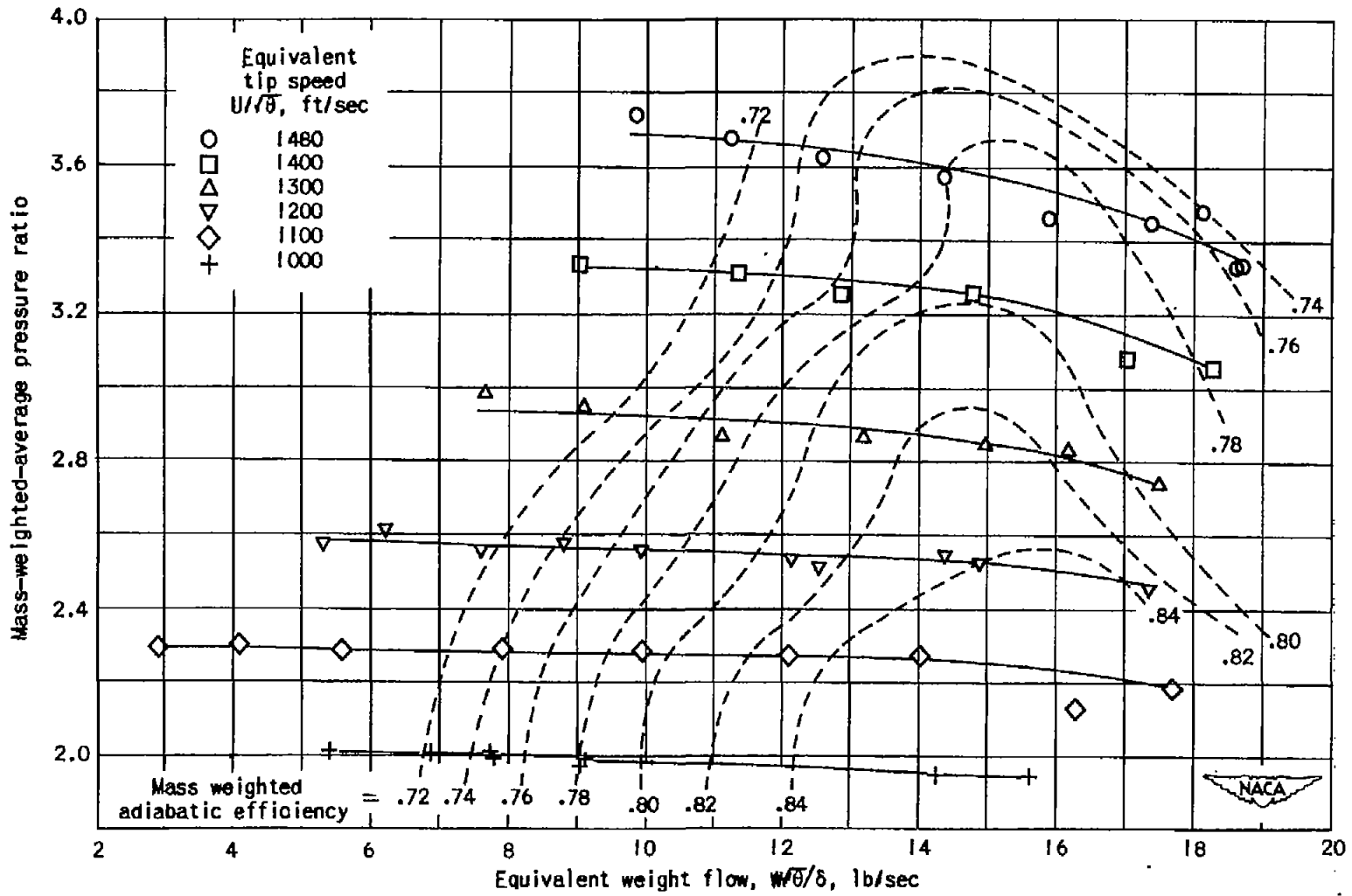


Figure 8. - Over-all performance of axial-discharge mixed-flow impeller.

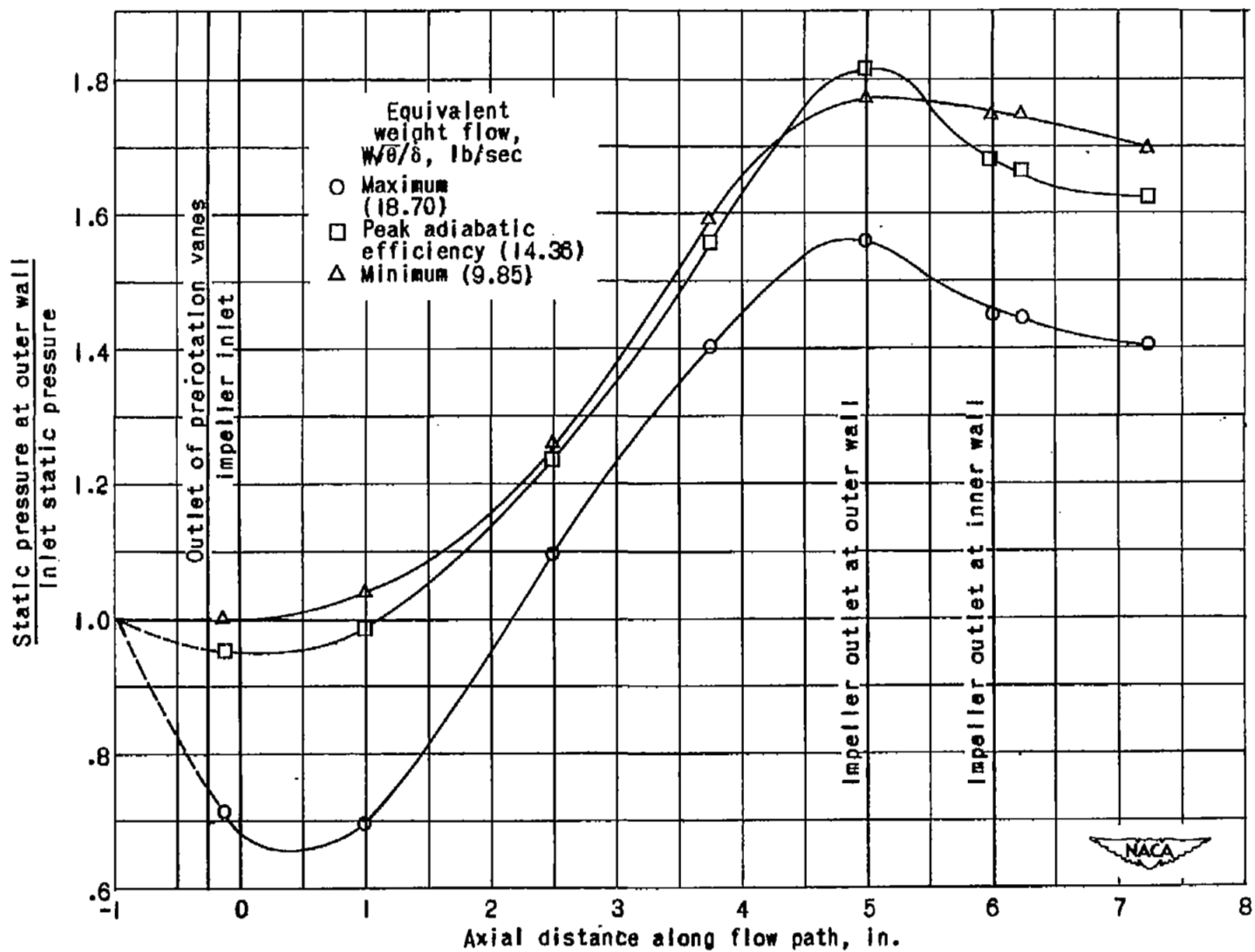


Figure 9. - Variation of static pressure along flow path at equivalent tip speed of 1480 feet per second. (Outer wall only.)

NASA Technical Library



3 1176 01435 5300